Korean J. Chem. Eng., 39(4), 887-901 (2022)
DOI: 10.1007/s11814-021-1004-0

pISSN: 0256-1115
eISSN: 1975-7220

Natural convection in F-shaped cavity filled with Ag-water non-Newtonian nanofluid saturated with a porous medium and subjected to a horizontal periodic magnetic field

Ahmed Kadhim Hussein*, Hameed Kadhem Hamzah*, Farooq Hassan Ali*, and Masoud Afrand,†**

*College of Engineering, Mechanical Engineering Department, University of Babylon, Babylon City, Hilla, Iraq
**Department of Mechanical Engineering, Najafabad Branch, Islamic Azad University, Najafabad, Iran
(*Received 13 March 2021 • Revised 10 October 2021 • Accepted 2 November 2021*)

Abstract−Natural convection in an F-shaped cavity containing Ag-water non-Newtonian nanofluid (NF) saturated with a porous medium was investigated numerically. The left wall of the cavity was maintained at a constant hot temperature and subjected to a horizontal periodic magnetic field. The right wall was maintained at a constant cold temperature. Both the top and bottom walls of the cavity were kept thermally insulated. In the present work, the Hartmann number varied as ($0 \le Ha \le 60$), the power law index varied as ($0.6 \le n \le 1.4$), the periodic shape parameter varied as ($0.1 \le \lambda \le 1$), the Rayleigh number varied as ($10^3 \le Ra \le 10^6$), the aspect ratio of the cavity varied as ($0.1 \le AR \le 0.4$), the Darcy number varied as ($10^{-5} \le Da \le 10^{-1}$) and the solid volume fraction varied as ($0 \le \varphi \le 0.06$). It was found that the average Nusselt number (Nu) increases by increasing the (φ, Da and Ra), whereas it decreases when (n) and (Ha) increase. Furthermore, it was realized that the relationship between the (Nu) and (λ) exhibits a different behavior depending on the considered values of (Ra) and (n).

Keywords: Natural Convection, Nanofluid, F-Shaped Cavity, Porous Medium, Non-Newtonian Fluid, Periodic Magnetic Field

INTRODUCTION

Most common coolants, such as ethylene glycol, oil and water, suffer from low thermal conductivity and, in consequence, their utilization in the heat transfer systems is not efficient enough to improve their performance [1-3]. This challenge can be solved by adding some solid nano-sized particles to these fluids. The suspension of the solid nanoparticle in the base fluid is called nanofluid (NF). These smart fluids are capable of augmenting the performance of heat transfer systems through their high thermal conductivity [4-6]. After the introduction of (NF), many researchers have studied their performance in various systems and reported the high potential of these modern coolants to replace common ones [7-11]. Another method suggested to improve the effectiveness of thermal equipment is the use of porous materials that have high thermal conductivity and exhibit a significant increase in the heat exchange surface area [12-15]. On the other hand, a magnetic field can be employed efficiently to control convective heat transfer inside the cavities. There are many practical applications of MHD natural convection, such as crystal growth in liquids, fire research, metallurgy and astrophysics [16,17].

Nowadays, naturally cooled irregular cavities have many uses in engineering and industry, such as air conditioning, thermal design of buildings, solar collectors, and cooling of electronic circuit boards. Many researchers have investigated this problem in these cavities such as L-shaped [18-21], inversed L-shaped [22], C-shaped [23-25], T-shaped [26,27], inversed T-shaped [28], -shaped [29], U-shaped [30], V-shaped [31], F-shaped [32], parabolic [33] and parallelogrammical [34]. The cooling performance of non-Newtonian (NFs) within naturally cooled cavities has been investigated by many researchers. Kefayati [35] employed the Lattice-Boltzmann technique to simulate the natural convection of non-Newtonian Cu-water (NF) in an enclosure. The impacts of (a, φ and n) were investigated. They highlighted the growth of heat transfer by boosting (n) and decreasing both (Ra) and (φ). Kefayati [36] numerically evaluated the effect of porous medium on the performance of a square cavity containing non-Newtonian aqueous Cu (NF). It was concluded that the increase of (φ, Ra and Da) entailed an intensification in (Nu). The impact of the external horizontal magnetic field on the hydro-thermal features of non-Newtonian Cu-water (NF) inside a naturally cooled cavity was evaluated by Kefayati [37]. The reduction of (Nu) by boosting (Ha) and (n) was reported. Wang et al. [38] numerically assessed the double-diffusive natural convection of non-Newtonian Cu-water (NF) in a rectangular cavity. It was depicted that (Nu) increased with the increment of (φ) and the decrement of (n). The effect of the magnetic field on the natural convection of non-Newtonian Cu-water (NF) in a rectangular cavity was determined by Wang et al. [39]. It was observed that (Nu) decreased with intensifying (n) and (Ha). Kefayati and Che Sidik [40] used the Lattice-Boltzmann technique to analyze the performance features of a naturally cooled square cavity containing non-Newtonian (NF). The effects of (n), cavity inclination angle and (Ra) were studied. They concluded that the increase of (n), cavity inclination angle and (Ra) exhibited an increment in (Nu). Raizah et al. [41] numerically simulated the unsteady natural convection of non-Newtonian Cu-water (NF) within an angled porous

†To whom correspondence should be addressed.
E-mail: masoud_afrand@yahoo.com
Copyright by The Korean Institute of Chemical Engineers.

open shallow enclosure. They concluded that (Nu) decreased by boosting (n), while it increased by boosting (Ra). The performance features of a naturally cooled cavity containing non-Newtonian Ag-water (NF) saturated with a porous medium were numerically investigated by Al-Amir et al. [42]. It was observed that the (Nu) increased with increasing (Da) and decreasing (n). Jabbar et al. [43] numerically investigated the impact of a sinusoidal interface wall on the performance features of a square enclosure containing non-Newtonian Ag-water (NF) saturated with a porous medium. They deduced that the (Nu) increased with the increase of (n). Very recently, Wang et al. [44] numerically assessed the impact of variable properties of shear thinning Al_2O_3-water (NF) on the performance of a naturally cooled enclosure. They deduced that (Nu) decreased with increasing (n). While the problem of the natural convection in irregular cavities containing a non-Newtonian (NF) was investigated by a second set of researchers. Alsabery et al. [45] numerically considered the visualization of heat lines for the natural convection of four non-Newtonian (NFs) in a trapezoidal porous cavity. The evaluated (NFs) were TiO_2-water, Al_2O_3-water, Cu-water, and Ag-water. They concluded that the highest (Nu) belonged to Ag-water (NF). The unsteady natural convection in a trapezoidal cavity containing a non-Newtonian (NF) was analyzed by Alsabery et al. [46]. Four types of nanoparticles were used (TiO_2, Al_2O_3, Cu and Ag), while the water was utilized as a base fluid. They realized that the increase of (φ) and sidewall inclination angle entailed an intensification in (Nu). Hatami [47] numerically explored natural convection in a square cavity containing non-Newtonian aqueous magnetite (NF) under the influence of a magnetic field with different inclination angles. He realized that the (Nu) decreased by increasing (Ha). Very recently, Acharya and Dash [48] numerically investigated MHD natural convection in a square wavy cavity containing non-Newtonian CuO-water (NF). They concluded that the non-Newtonian aspect of (NF) entailed (15%) increase in the (Nu). Other useful references can be found in Refs. [49,50].

Researchers have used both laboratory and numerical methods in the field of nanofluids to conduct their research [51-55]. Some researchers have used numerical methods for their studies due to their lower cost and speed [55-60]. In contrast, other researchers have used the laboratory method due to its high accuracy [61-65]. Many researchers in recent years have used nanofluids and pointed out its importance [66-70]. According to our best knowledge in this field and depending upon the above literature review, it can be mentioned that natural convection in F-shaped cavity containing Ag-water non-Newtonian (NF) saturated with a porous medium and subjected to a horizontal periodic magnetic field was not considered in any paper to date. Therefore, the aim of this contribution is to assess this problem in detail.

PHYSICAL MODEL DESCRIPTION AND GOVERNING EQUATIONS

Fig. 1 displays the geometry and imposed boundary conditions of the considered problem in the current assessment. It is seen that the studied geometry is a two-dimensional F-shaped cavity filled with an NF-saturated porous medium. The left and right walls of cavity are kept at a constant temperature (T_h and T_c<T_h, respectively),

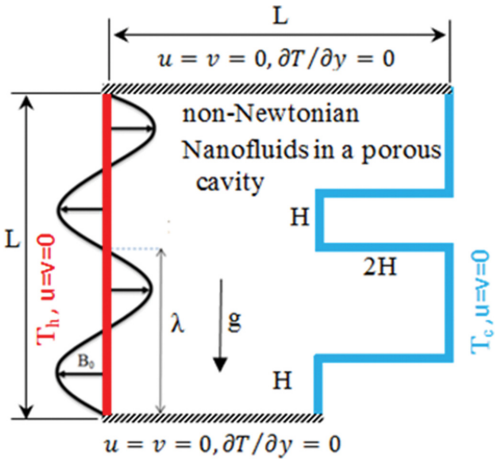


Fig. 1. Schematic diagram of the present problem.

while both the top and bottom walls are insulated. A periodic magnetic field with amplitude of (B_0) and wave length of (λ) ($\vec{\dot{B}} = \vec{\dot{B}}_o \sin\left(\frac{\pi y}{\lambda}\right)$) is applied to the left straight wall of the cavity. No-slip boundary condition on solid walls is used ($\dot{u} = \dot{v} = 0$). The employed (NF) is the non-Newtonian shear thinning Ag-water (NF).

1. Governing Formulas

Several models have been presented in the literature to determine the hydro-thermal aspects of fluid flow inside a porous medium, including Darcy, Darcy-Brinkman and Darcy-Forchheimer models [71]. Among these, the Darcy-Brinkman model has received more attention due to the inclusion of drag force of solid phase in the equation of momentum. In the present study, considering the following assumptions, this method has been used to perform numerical tasks.

- The flow is laminar, incompressible, and steady.
- Apart from density, other properties of (NF) are constant. The Boussinesq approximation is employed to determine the variation of density with temperature.
- Thermal equilibrium is considered between water and nanoparticles as well as between porous medium and (NF).
- The porous medium is considered isotropic.
- Viscous dissipation and radiation effects are negligible.

The considered governing formulas in the current work are the conservation of mass, momentum, and energy, respectively [72]:

$$\frac{\partial \dot{u}}{\partial x} + \frac{\partial \dot{v}}{\partial y} = 0 \tag{1}$$

$$\dot{u}\frac{\partial \dot{u}}{\partial x} + \dot{v}\frac{\partial \dot{u}}{\partial y} = -\frac{1}{\rho_{na}}\frac{\partial \dot{p}}{\partial x} + \frac{1}{\rho_{na}}\left(\frac{\partial \dot{\tau}_{xx}}{\partial x} + \frac{\partial \dot{\tau}_{xy}}{\partial y}\right) - \frac{\dot{v}_{na}}{\dot{K}}\dot{u} \tag{2}$$

$$\dot{u}\frac{\partial \dot{v}}{\partial x} + \dot{v}\frac{\partial \dot{v}}{\partial y} = -\frac{1}{\rho_{na}}\frac{\partial \dot{p}}{\partial y} + \frac{1}{\rho_{na}}\left(\frac{\partial \dot{\tau}_{xy}}{\partial x} + \frac{\partial \dot{\tau}_{yy}}{\partial y}\right) + g\beta_{na}(\dot{T} - \dot{T}_c) - \frac{\dot{v}_{na}}{\dot{K}}\dot{v} + \sigma_{na}B^2\dot{v} \tag{3}$$

$$\dot{u}\frac{\partial \dot{T}}{\partial x} + \dot{v}\frac{\partial \dot{T}}{\partial y} = \alpha_{na}\left(\frac{\partial^2 \dot{T}}{\partial x^2} + \frac{\partial^2 \dot{T}}{\partial y^2}\right) \tag{4}$$

To transform Eqs. (1)-(4) from dimensional form to dimensionless form to progress the numerical solution, the next dimensionless parameters must be defined [36]:

$$X=\frac{x}{L},\ Y=\frac{y}{L},\ \dot{U}=\frac{\dot{u}}{\left(\frac{\alpha_{bf}}{L}\right)\sqrt{Ra}},\ \dot{V}=\frac{\dot{v}}{\left(\frac{\alpha_{bf}}{L}\right)\sqrt{Ra}},\ \dot{P}=\frac{\dot{p}}{\rho_{na}\left(\frac{\alpha_{bf}}{L}\right)^2 Ra},$$

$$\dot{\theta}=\frac{\dot{T}-T_c}{T_h-T_c},\ Ra=\frac{\rho_{bf}\beta_{bf}gL^3(T_h-T_c)}{\mu_{bf}\alpha_{bf}},\ Pr=\frac{\mu_{bf}}{\rho_{bf}\alpha_{bf}},\ Da=\frac{K}{L^2},$$

$$Ha=LB\sqrt{\frac{\sigma}{\mu_{bf}}} \tag{5}$$

The dimensionless forms of the governing formulas are as follows:

$$\frac{\partial\dot{U}}{\partial X}+\frac{\partial\dot{V}}{\partial Y}=0 \tag{6}$$

$$\dot{U}\frac{\partial\dot{U}}{\partial X}+\dot{V}\frac{\partial\dot{U}}{\partial Y}=-\frac{\partial\dot{P}}{\partial X}+\frac{Pr}{\sqrt{Ra}}\frac{\rho_{bf}}{\rho_{na}}\frac{1}{(1-\varphi)^{2.5}}\left[2\frac{\partial}{\partial X}\left(\frac{\mu_{bf}}{N}\frac{\partial\dot{U}}{\partial X}\right)+\frac{\partial}{\partial Y}\left(\frac{\mu_{bf}}{N}\left(\frac{\partial\dot{U}}{\partial Y}+\frac{\partial\dot{V}}{\partial X}\right)\right)\right]$$
$$-\frac{\rho_{bf}}{\rho_{na}}\frac{1}{(1-\varphi)^{2.5}}\frac{Pr}{Da\sqrt{Ra}}\frac{\mu_{bf}}{N}\dot{U} \tag{7}$$

$$\dot{U}\frac{\partial\dot{V}}{\partial X}+\dot{V}\frac{\partial\dot{V}}{\partial Y}=-\frac{\partial\dot{P}}{\partial Y}+\frac{Pr}{\sqrt{Ra}}\frac{\rho_{bf}}{\rho_{na}}\frac{1}{(1-\varphi)^{2.5}}\left[2\frac{\partial}{\partial Y}\left(\frac{\mu_{bf}}{N}\frac{\partial\dot{U}}{\partial Y}\right)+\frac{\partial}{\partial X}\left(\frac{\mu_{bf}}{N}\left(\frac{\partial\dot{U}}{\partial Y}+\frac{\partial\dot{V}}{\partial X}\right)\right)\right]$$
$$+Pr\frac{(\rho\beta)_{na}}{\rho_{na}\beta_{bf}}\dot{\theta}-\frac{\rho_{bf}}{\rho_{na}}\frac{1}{(1-\varphi)^{2.5}}\frac{Pr}{Da\sqrt{Ra}}\frac{\mu_{bf}}{N}\dot{V}$$
$$+\frac{\rho_{bf}}{\rho_{na}}\frac{1}{(1-\varphi)^{2.5}}\frac{\sigma_{na}}{\sigma_{bf}}\frac{PrHa^2}{\sqrt{Ra}}B\dot{V} \tag{8}$$

$$\dot{U}\frac{\partial\dot{\theta}}{\partial X}+\dot{V}\frac{\partial\dot{\theta}}{\partial Y}=\frac{1}{\sqrt{Ra}}\frac{\alpha_{na}}{\alpha_{bf}}\left(\frac{\partial^2\dot{\theta}}{\partial X^2}+\frac{\partial^2\dot{\theta}}{\partial Y^2}\right) \tag{9}$$

Concerning the case study specification and dimensionless variables, the boundary conditions of the present work are specified as follows:

$$\dot{\theta}=1;\ \dot{U}=\dot{V}=0;\ X=0;\ 0\le Y\le 1;\ \text{Left side wall} \tag{10a}$$

$$\dot{\theta}=0;\ \dot{U}=\dot{V}=0;\ X=1;\ 0\le Y\le 1;\ \text{Right side wall} \tag{10b}$$

$$\frac{\partial\dot{\theta}}{\partial Y}=0;\ \dot{U}=\dot{V}=0;\ Y=1;\ 0\le X\le 1;\ \text{Top wall} \tag{10c}$$

$$\frac{\partial\dot{\theta}}{\partial Y}=0;\ \dot{U}=\dot{V}=0;\ Y=0;\ 0\le X\le 1;\ \text{Bottom wall} \tag{10d}$$

The thermo-physical aspects of silver-water (NF) are computed from the following formulas [36]:

$$\rho_{na}=(1-\varphi)\rho_{bf}+\varphi\rho_{so} \tag{11}$$

$$\alpha_{na}=k_{na}/(\rho C_p)_{na} \tag{12}$$

$$(\rho C_p)_{na}=(1-\varphi)(\rho C_p)_{bf}+\varphi(\rho C_p)_{so} \tag{13}$$

$$(\rho\beta)_{na}=(1-\varphi)(\rho\beta)_{bf}+\varphi(\rho\beta)_{so} \tag{14}$$

Table 1. Thermo-physical properties of water and silver nanoparticles [32]

Property	Water	Silver nanoparticle
ρ (kg/m^3)	997.1	1,050
C_p (J/kg K)	4,179	235
k (W/m·K)	0.613	429
$\beta\times10^5$ (1/K)	21	5.9
σ (S/m)	0.05	6.3×10^{-7}

$$\frac{\sigma_{na}}{\sigma_{bf}}=1+\frac{3\left(\frac{\sigma_{so}}{\sigma_{bf}}-1\right)\varphi}{\left(\frac{\sigma_{so}}{\sigma_{bf}}+2\right)-\left(\frac{\sigma_{so}}{\sigma_{bf}}-1\right)\varphi} \tag{15}$$

$$\frac{k_{na}}{k_{bf}}=\frac{(1-\varphi)(k_{so}+2k_{bf})+3\varphi k_{so}}{(1-\varphi)(k_{so}+2k_{bf})+3\varphi k_{bf}} \tag{16}$$

$$\mu_{na}=\frac{\mu_{bf}}{(1-\varphi)^{2.5}} \tag{17}$$

where

$$\mu_{bf}=N\left\{2\left[\left(\frac{\partial\dot{u}}{\partial x}\right)^2+\left(\frac{\partial\dot{u}}{\partial y}\right)^2\right]+\left(\frac{\partial\dot{v}}{\partial x}+\frac{\partial\dot{u}}{\partial y}\right)^2\right\}^{\frac{(n-1)}{2}} \tag{18}$$

The thermo-physical properties of water and sliver nanoparticles are reported in Table 1.

The rheological behavior of fluids is a function of (n) so that if =1, n>1 and n<1, the fluid is Newtonian, non-Newtonian shear-thinning and non-Newtonian shear thickening, respectively.

In the present study, the stream function is used to represent the velocity components. The relationship between the stream function and the velocity components is as follows:

$$\dot{U}=\frac{\partial\Psi}{\partial Y};\ \dot{V}=-\frac{\partial\Psi}{\partial X} \tag{19}$$

$$\nabla^2\Psi=\frac{\partial\dot{U}}{\partial Y}-\frac{\partial\dot{V}}{\partial X} \tag{20}$$

The rate of heat transfer is calculated by using the local and mean (Nu) of the left hot wall, which are computed as follows:

$$Nu_l=\left(-\frac{\partial\dot{\theta}}{\partial X}\right)_{X=0} \tag{21}$$

$$Nu_{ave}=\int_0^1 Nu_l dy \tag{22}$$

NUMERICAL METHOD AND VERIFICATION

The system of governing equations exposed to the above-mentioned boundary conditions is solved employing Galerkin-finite element technique. In this technique, weighted residual method is employed to transform the non-linear partial differential equations into linear system of equations [71]. Fig. 2 represents the meshing of the computational domain employed in the current assessment. Given that the present work is a numerical study, it is necessary to determine the appropriate number of nodes, because the

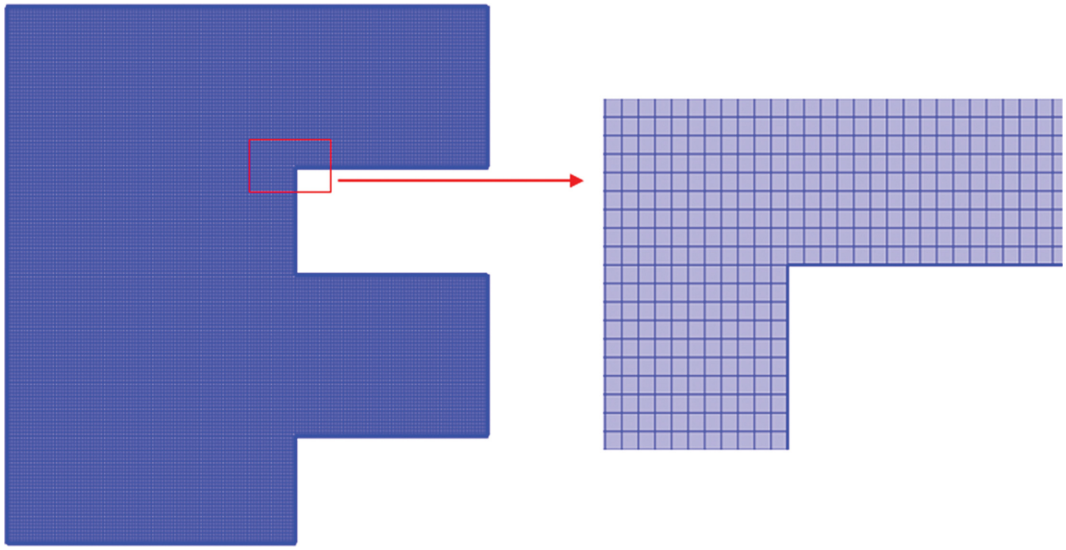


Fig. 2. Mesh distribution of the computational domain.

Table 2. Grid independent test for average Nussult number and ($|\Psi|_{max}$) on hot surface at (Ra=10^6, λ=0.5, φ=0.04, Ha=30, Da=0.001, AR=0.2 and n=0.6)

Grid size	Nu	$\Delta=\frac{\lvert Nu_{i\times j}-Nu_{200\times 200}\rvert}{Nu_{i\times j}}\times 100$	$\lvert\Psi\rvert_{min}$	$\Delta=\frac{\lvert\Psi_{i\times j}-\Psi_{200\times 200}\rvert}{\Psi_{i\times j}}\times 100$
100×100	11.547	0.848	0.02214	0.585
150×150	11.621	0.206	0.02224	0.134
200×200	11.645	-	0.02227	-
250×250	11.654	0.077	0.02229	0.0897
300×300	11.659	0.042	0.02230	0.134

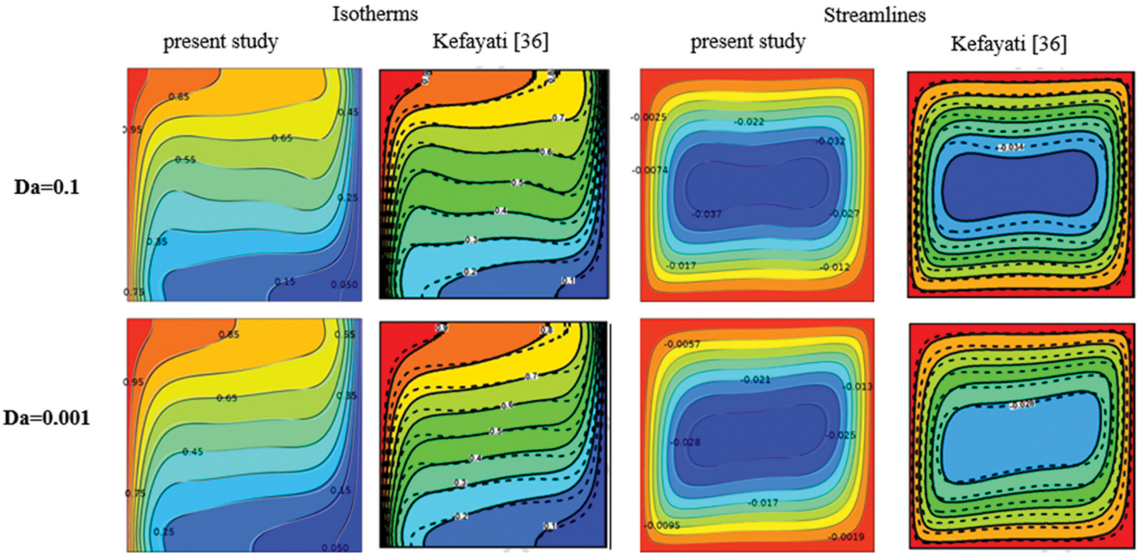


Fig. 3. Isotherms (left) and streamlines (right) comparison between the present study ((black lines φ=0), (grey lines φ=0.04)) and Kefayati [36] (base fluid (—) (φ=0) and nanofluids (---) (φ=0.04)) for various (Da) at (n=0.6 and Ra=10^5).

results should not change with changing the number of nodes. To this end, five different grids were prepared and simulations were performed using them. The results of validation are shown in Table 2. For the validation, the (Nu) and ($|\Psi|_{max}$) on the hot surface at (Ra=10^6, λ=0.5, φ=0.04, Ha=30, Da=0.001, AR=0.2 and n=0.6) were utilized. The findings illustrate that the grid size of 200×200

is suitable to conduct the simulations. Another important issue in the numerical research is validation. In this work, the findings of our home-made code were compared with the numerical findings of Kefayati [36] for natural convective heat transfer of non-Newtonian (NFs) in a porous square cavity. The comparison results are considered for both streamlines and isotherms as shown in Fig. 3. This comparison shows very good agreement between the two results and, therefore, our code is valid.

RESULTS AND DISCUSSION

This work is devoted to the numerical investigation of the natu-

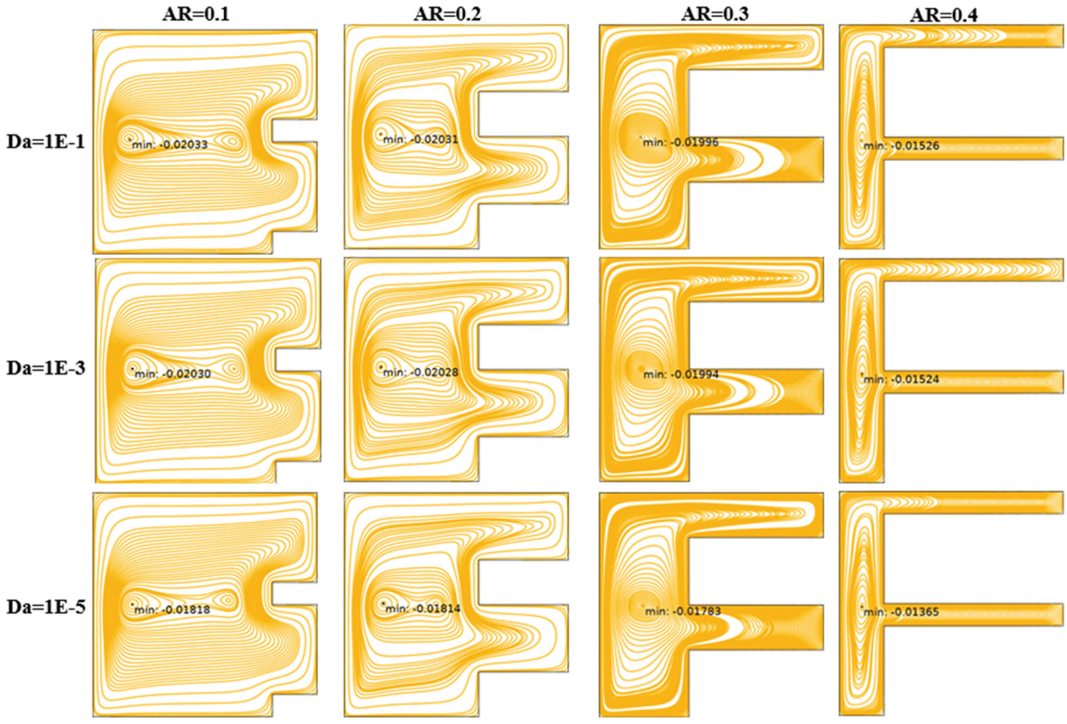


Fig. 4. Streamline contours for various values of (Da and AR) at (Ra=10^6, n=0.8, φ=0.04, Ha=30 and λ=0.5).

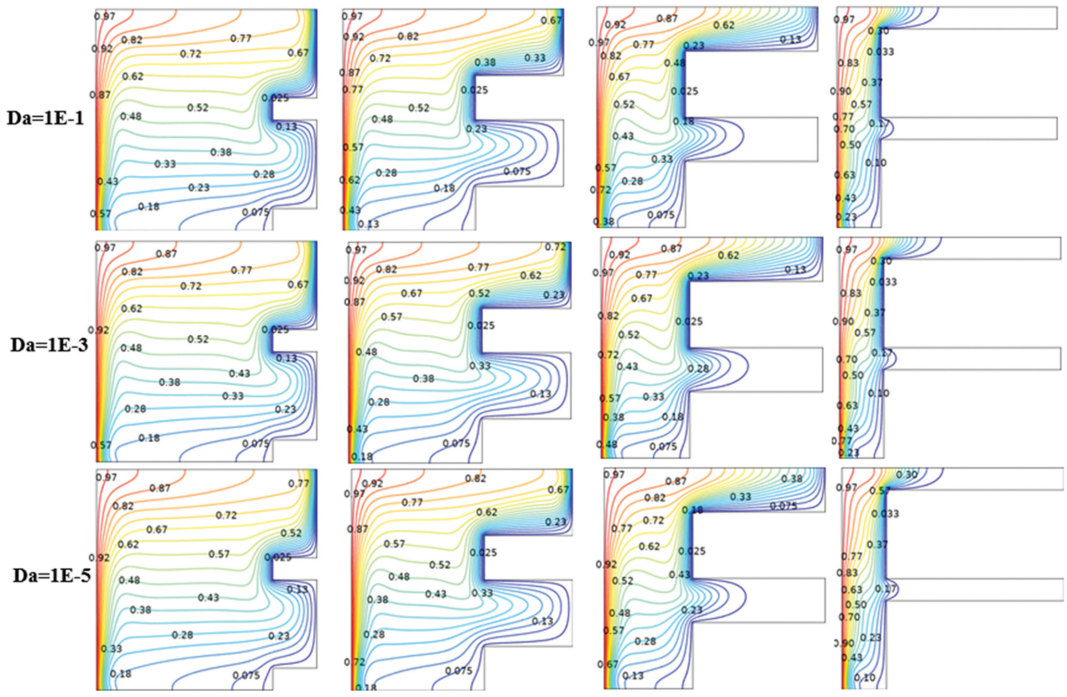


Fig. 5. Isotherm contours for various values of (Da and AR) at (Ra=10^6, n=0.8, φ=0.04, Ha=30 and λ=0.5).

ral convection of non-Newtonian Ag-water (NF) inside an F-shaped cavity in the presence of a periodic magnetic field. The effects of Ha (0-60), n (0.6-1.4), λ (0.1-1), Ra (10^3-10^5), AR (0.1-0.4), Da (10^{-5}-10^{-1}) and φ (0-0.06) on the outcomes were investigated.

1. Effects of AR and Da

The streamline and isotherm contours in terms of (AR) and (Da) at Ra=10^6, n=0.8, φ=0.04, Ha=30 and λ=0.5 are, respectively, illustrated in Figs. 4 and 5. The flow field is initiated inside the F-shaped cavity next to the hot left wall and moves towards the adiabatic top wall. Physically, the fluid next to the hot left wall heats up and, as a result, expands upward. After that, it cools by passing next to the cold right wall before it reaches the adiabatic bottom wall. Due to this cooling, the fluid begins to compress and moves downward. This cyclic motion of the flow entails the formation of vortices. The formation of flow vortices is caused by the temperature difference between cold and hot sidewalls. Fig. 4 depicts that for all the considered (Da), the values of the stream function decrease by increasing (AR). This behavior can be seen for all considered values of the Darcy number. For example, at (Da=10^{-1}) the stream function decreases from (0.02033) at (AR=0.1) to (0.01526) at (AR=0.4). Therefore, it can be concluded that the flow circulation strength decreases with the increase of (AR). This is due to the increment of internal cold rib inside the cavity by boosting the (AR), which entails the restriction of motion of the flow vortices, and as a result, the flow circulation begins to decline. Also, Fig. 4 shows that the size of flow vortices decreases as the (AR) increases. In addition, the pattern of vortices changes markedly with increasing (AR). Since, they switch their horizontal pattern for low (AR) to the vertical one for high (AR). Besides, Fig. 4 shows that the stream function values decline as the (Da) decreases from (10^{-1}) to (10^{-5}). For example, at (AR=0.1), the stream function declines from (0.02033) at (Da=10^{-1}) to (0.01818) at (Da=10^{-5}). The increase in the Darcy number entails an increase in the permeability of porous medium and reduces its resistance to the flow field. Therefore, the vortices move faster inside the cavity and, as a result, the stream function value increases. Fig. 5 demonstrates the effect of

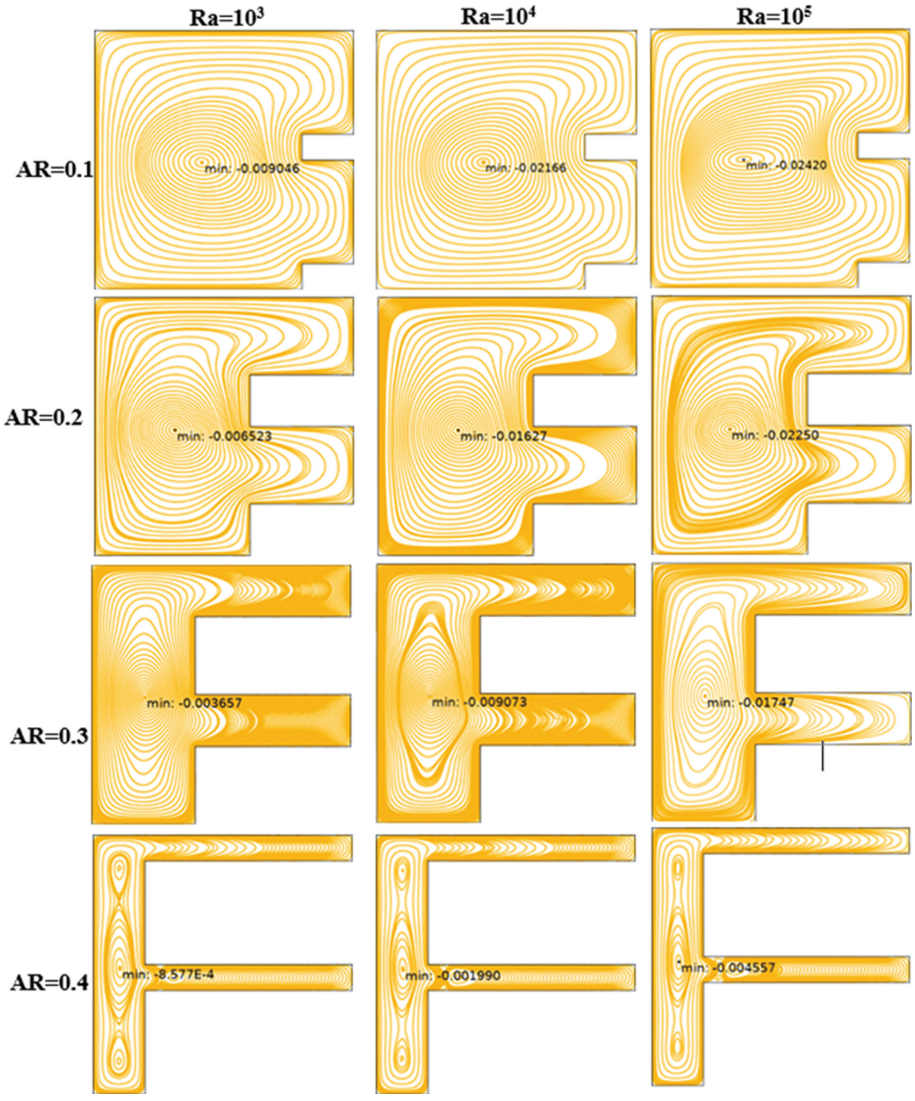


Fig. 6. Streamline contours for various values of (Ra and AR) at (Da=10^{-3}, n=0.6, φ=0.04, Ha=30 and λ=0.5).

(AR) and (Da) on the isotherm contours. It is observed that, at (AR=0.1), the isotherms are distributed freely through the cavity. This helps them to transfer more energy between the hot and cold fluids and makes convective heat transfer faster. But at (AR=0.4), a clear restriction in the heat transfer zone is seen. In this case, the effect of natural convection between the hot and cold sidewalls decreases significantly. This can originate from the stagnant zones in the cold rib region of the right sidewall, which weakens the flow circulation. Therefore, the isotherms seem to be symmetric and uniform, especially in the middle of the cavity, which indicates that conduction is the dominant heat transfer mechanism. Moreover, it is clear that at low values of (Da) (i.e., $Da=10^{-1}$), the isotherms are concentrated next to the hot and cold sidewalls. So, they leave these regions and move further to another region in the cavity. This is due to the strong flow circulation and the steep temperature gradient between the sidewalls, which makes the isotherms more confused especially in the middle of cavity. Therefore, convective heat transfer is dominant when (Da) is high. But, as (Da) decreases to (10^{-5}), the isotherms become more uniform and linear, especially in the middle of the cavity. In this case, the temperature distribution becomes similar to that noticed for a stationary fluid and the heat transfer inside the cavity occurs by conduction.

2. Effects of Ra and AR

The streamline and isotherm contours in terms of (Ra) and (AR) at $Da=10^{-3}$, n=0.6, φ=0.04, Ha=30 and λ=0.5 are, respectively, illustrated in Figs. 6 and 7. For all the studied cases, the increase of (Ra) entails an intensification in the stream function values. The results show that at ($Ra=10^3$), the flow circulation is very weak and the pattern of the rotating vortices is symmetrical and uniform, especially in the cavity core. But, at ($Ra=10^5$), the stream function values increase and the shape of rotating vortices becomes asymmetric. As (Ra) increases, the buoyancy force and, therefore, the flow circulation strength intensifies. Fig. 6 depicts that the values of stream function decrease with increasing (AR). For example, at ($Ra=10^5$), the stream function values decline from (0.02420) at (AR=0.1) to (0.004557) at (AR=0.4).

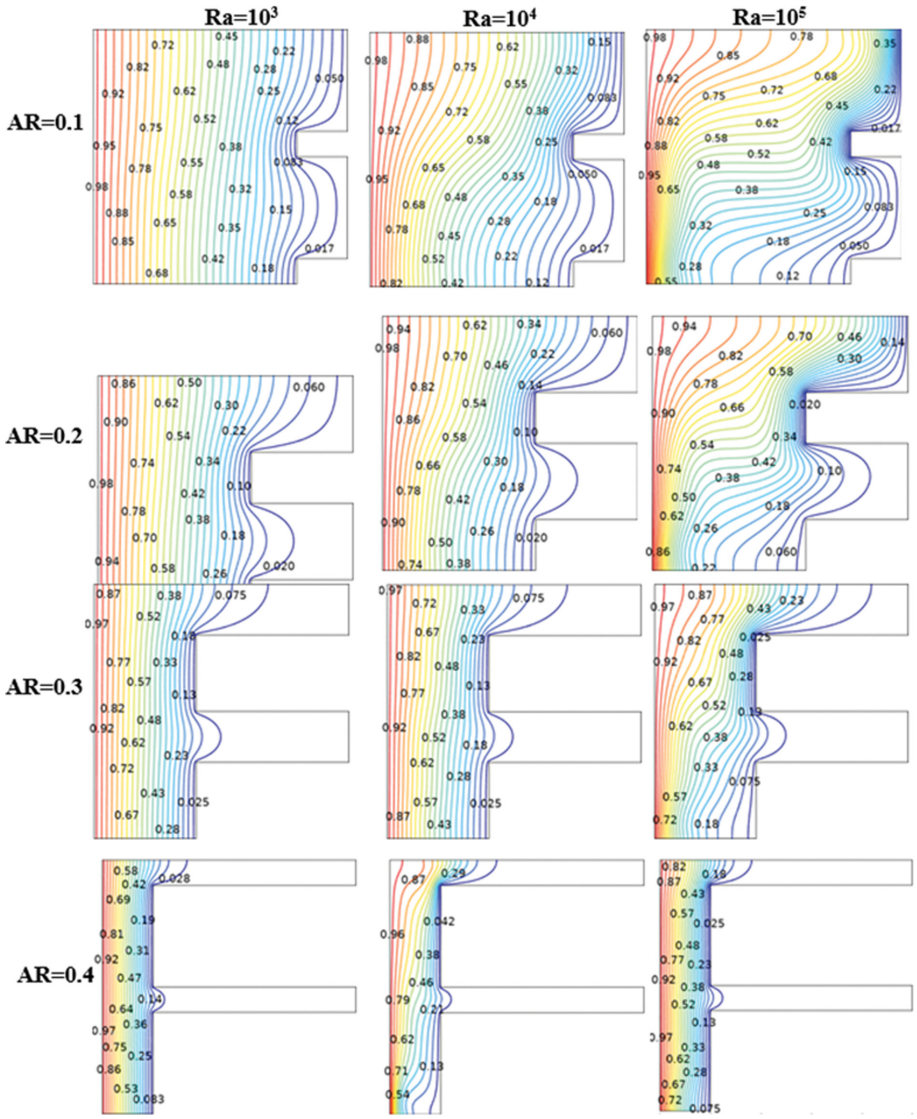


Fig. 7. Isotherm contours for various values of (Ra and AR) at ($Da=10^{-3}$, n=0.6, φ=0.04, Ha=30 and λ=0.5).

Fig. 7 demonstrates that at ($a=10^3$), the isotherm lines are symmetrical and parallel to the cavity sidewalls. This is due to the weak buoyancy force, which makes conduction the main mechanism of heat transfer. Whereas, at ($Ra=10^5$), convection is dominant instead of the conduction. This can be evident from the strong distortion of the isotherm lines at ($Ra=10^5$) compared with their pattern at ($Ra=10^3$). Also, at ($Ra=10^5$), an intense accumulation of the isotherm lines near the hot left sidewall of the cavity can be seen, which originated as a result of the high temperature gradient in this region. Moreover, Fig. 7 reveals that the isotherm lines are clearly influenced by boosting (AR). They changed their pattern from curved and confused shape, especially at ($Ra=10^5$) when the

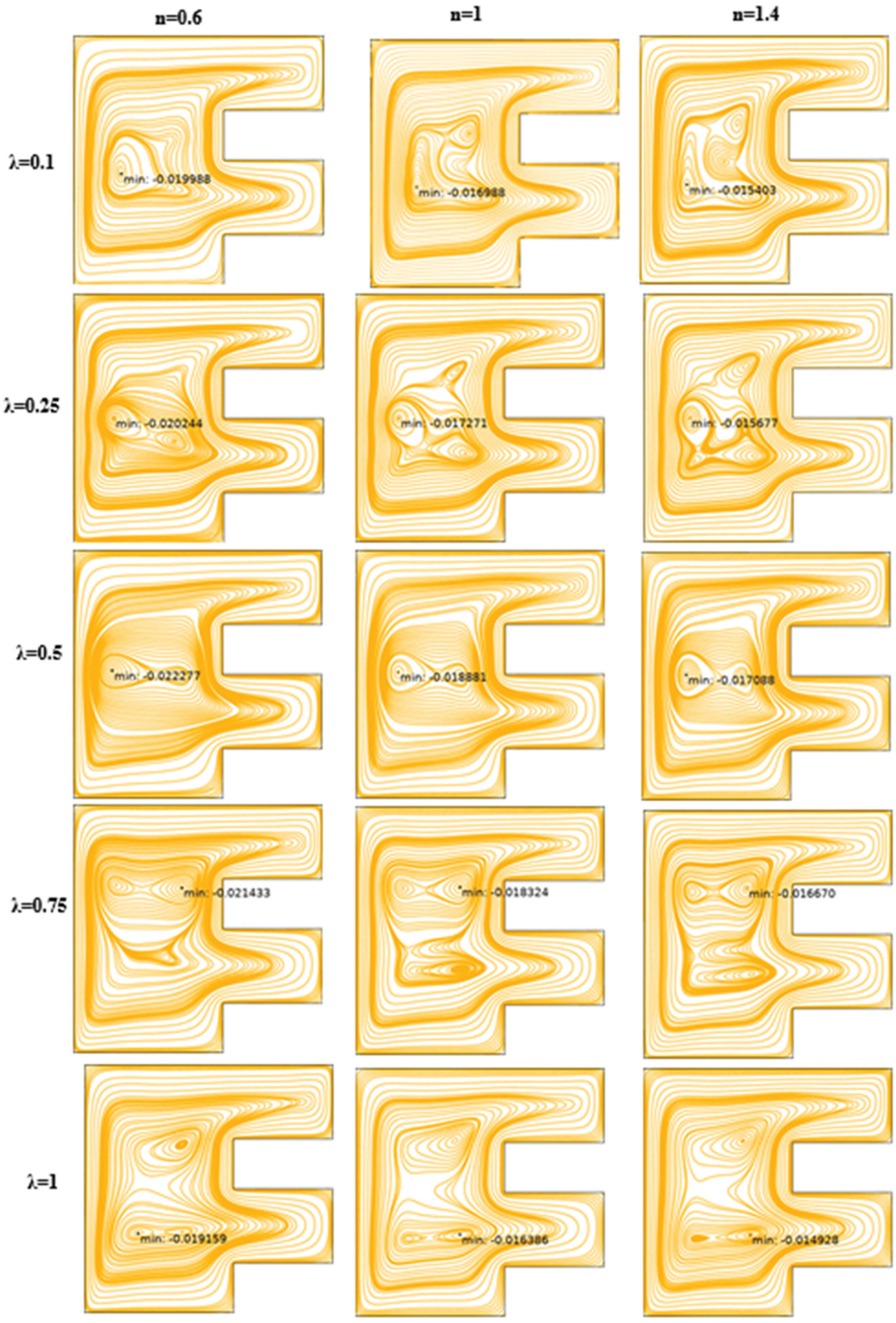


Fig. 8. Streamline contours for various values of (n and λ) at ($Da=10^{-3}$, $Ra=10^6$, φ=0.04, Ha=30 and AR=0.2).

(AR) is low (i.e., AR=0.1) to a parallel and uniform pattern when (AR) is high (i.e., AR=0.4). Therefore, the increase of (AR) entails the change of main mechanism of heat transfer from convection to conduction.

3. Effects of n and λ

The streamline and isotherm contours in terms of (n) and (λ) at (Da=10^{-3}, Ra=10^{6}, φ=0.04, Ha=30 and AR=0.2) are, respectively, displayed in Figs. 8 and 9. It is evident that for all the stud-

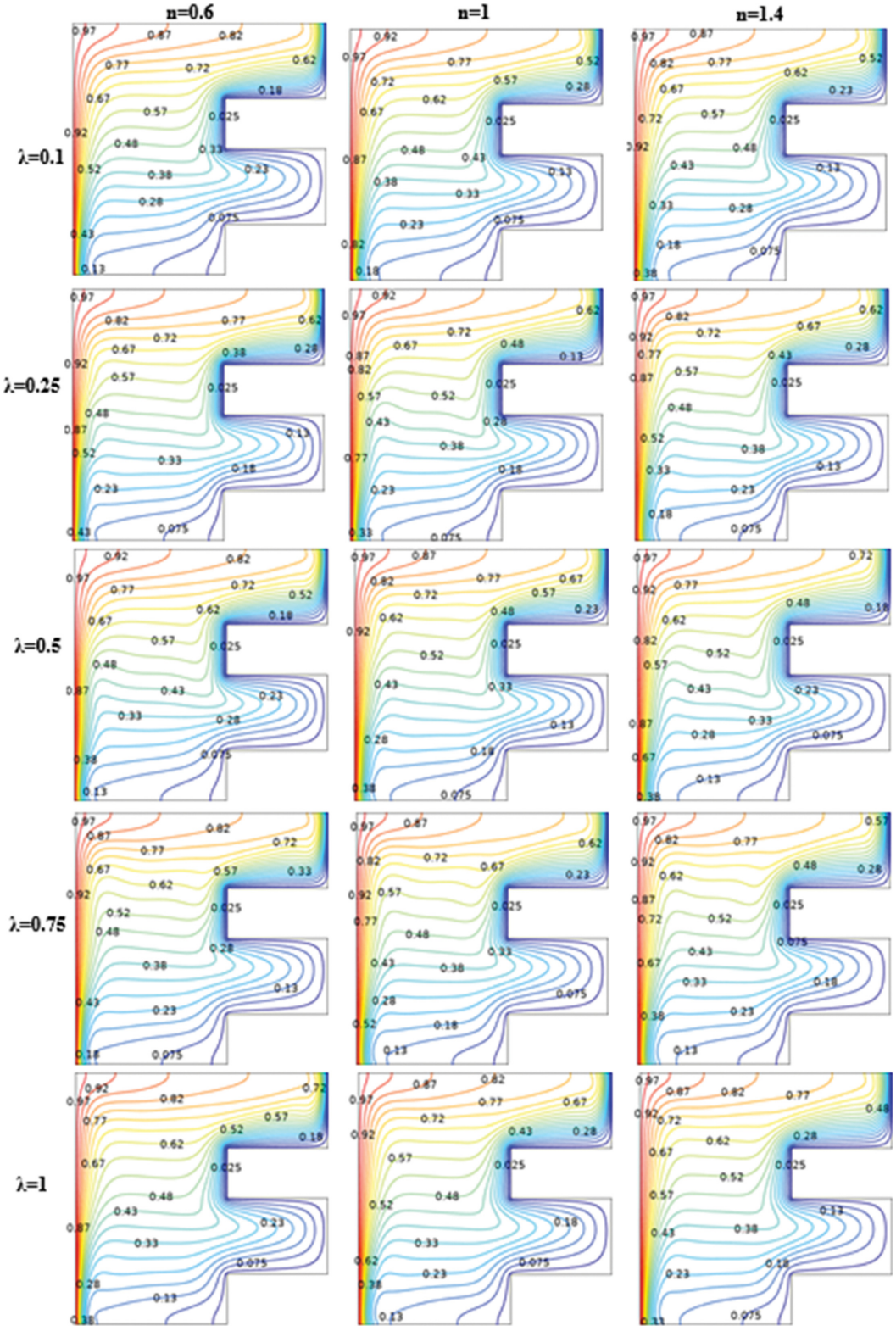
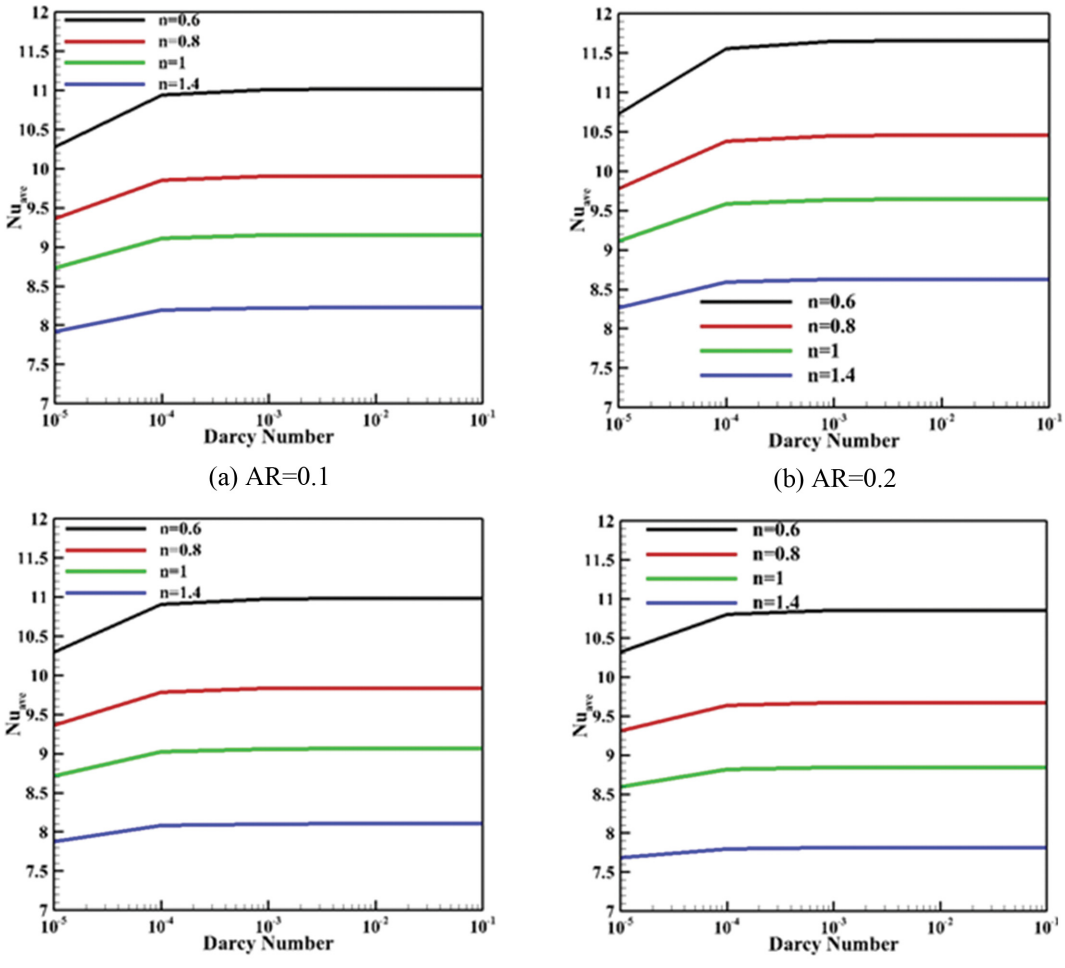


Fig. 9. Isotherm contours for various values of (n and λ) at (Da=10^{-3}, Ra=10^{6}, φ=0.04, Ha=30 and AR=0.2).

ied values of (λ), the stream function values decrease by increasing (n). For instance, at (λ=0.25), the stream function value goes from (0.020244) at (n=0.6) to (0.015677) at (n=1.4). The increment of (n) entails an increase in the (NF) viscosity, which causes a rise in the stream function values. On the other hand, due to the increased viscosity of (NF), the rotation of the (NF) is significantly attenuated. Fig. 8 also shows that the flow field pattern is affected significantly by boosting (λ). At low (λ, i.e λ=0.1), the effect of the periodicity of the magnetic field on the flow field is very small and, as a result, the flow field is similar to the uniform magnetic field state (i.e., λ=0). At (λ=0.1), the Lorentz force component along the y-axis is much more efficient than its other components. This causes a clear confusion in the streamline pattern, especially in the cavity core. With the increase of (λ) from (0 to 0.25 and 0.5), the magnetic field begins to be periodic and an intensification in the stream function value can be seen compared with the case of (λ=0.1). For instance, at (n=0.6), the stream function value increases from (0.01998) at (λ=0.1) to (0.022277) at (λ=0.5). This increase is due to the decrease of Lorentz force gradient along the y-axis, which weakens the magnetic field effect and, consequently, augments the flow circulation strength. Therefore, the streamlines switch their pattern from confused curved shape at (λ=0.1) to a straight uniform shape at (λ=0.5). Moreover, the increase in (λ) changes the direction of the rotating vortices core from the vertical at (λ=0.1) to horizontal at (λ=0.25 and 0.5). This leads to clearly squeezing the streamlines next to the hot left sidewall. But further increase in the λ to (0.75 and 1) entails a decline in the stream function values. For example, at (n=0.6), the stream function value goes from (0.021433) at (λ=0.75) to (0.019159) at (λ=1). Therefore, Fig. 8 depicts that as the (λ) value increases, the flow circulation strength first diminishes and then increases. Fig. 9 shows that, as the (n) increases, there are small changes in the isotherm contours. The only point which can be mentioned here is that the strength of isotherms next to the hot left sidewall begins to drop with boosting the (n). On the other hand, it is seen that when (λ) is low, the isotherms are uniform and parallel to the top and bottom walls of cavity. This is due to the effect of the magnetic field, which is similar to a uniform magnetic field state. In this case, the conduction heat transfer is dominant. Now, when (λ) increases to (λ=0.25 and 0.5), the isotherms begin to deviate, especially in the center of the cavity. They become more curved and more condensed to each other. Since, in this case, the magnetic field effect begins to decrease and,



(a) AR=0.1 (b) AR=0.2

(c) AR=0.3 (d) AR=0.4

Fig. 10. The changes of (Nu) in terms of (Da, n and AR) at (Ra=10^6, φ=0.04, Ha=30 and λ=0.5).

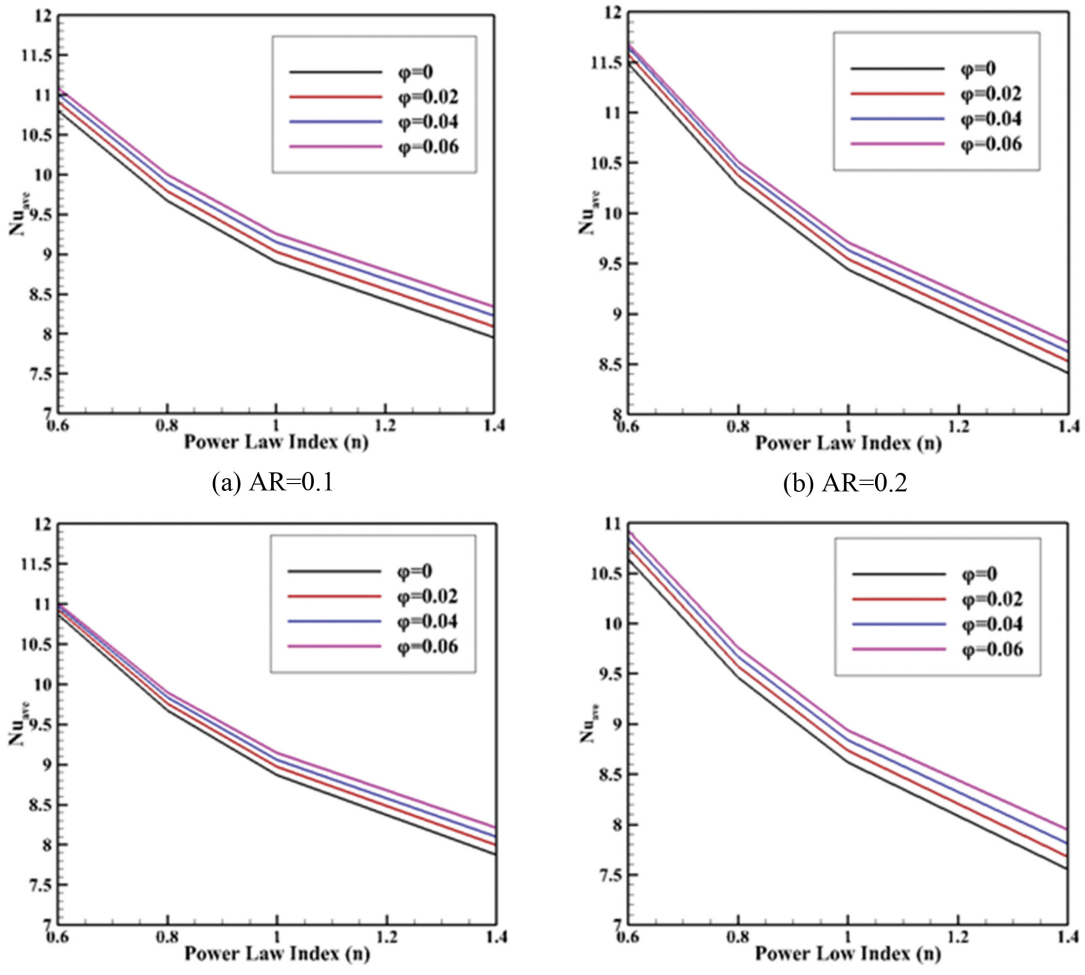
consequently, convective heat transfer is dominant. For further increase in the (λ) values to (0.75 and 1), the isotherm pattern returns again to its uniform and parallel state. The is because of the intensification of the magnetic field and, in consequence, the conduction heat transfer repeats its dominance again over the convection mechanism.

4. Average Nu

Fig. 10 illustrates the changes of (Nu) along the hot wall versus (Da), (n) and (AR) at (Ra=10^6, φ=0.04, Ha=30 and λ=0.5). As is seen, the (Nu) increases by boosting the (Da). Boosting the (Da) from (10^{-5} to 10^{-1}) exhibits an increment in the permeability of the porous medium, which leads to improved convective heat transfer and (Nu) within the cavity. In addition, (Nu) reaches its maximum value at (AR=0.2), which is due to the optimal distance between the cold and hot walls of the cavity at this (AR). Fig. 10 demonstrates that (Nu) decreases by increasing (n), which is because of the increment of (NF) viscosity and thermal boundary layer thickness. In consequence, it can be claimed that the rate of heat transfer for shear-thickening (NFs) (n>1) is lower than the shear-thinning (n<1) and Newtonian (n=1) (NFs).

The change of (Nu) against (n) in terms of (φ and AR) at (Ra=10^6, Da=0.001, Ha=30, and λ=0.5) is illustrated in Fig. 11. (Nu) increases by increasing (φ), which is because of the intensification of the (NF) thermal conductivity. Therefore, it can be said that the non-Newtonian silver-water (NF) is a better coolant than the pure water, especially at high (φ, i.e., φ=0.06). Moreover, it is observed that the highest (Nu) can be found at (AR=0.2). Furthermore, it can be noted from Fig. 11 that the (Nu) decreases as (n) increases. So, the highest (Nu) occurs at (φ=0.06 and n=0.6).

Fig. 12 displays the changes of (Nu) in terms of (Ha) and (AR) at (Ra=10^6, φ=0.04, Da=0.001 and λ=0.5). According to the findings, the increase of (Ha) entails a decline in (Nu). The implementation of a magnetic field leads to the application of Lorentz force to the fluid, which opposes the rotation of the fluid and boosts (Ha). This leads to the amplification of this force and, therefore, further reduction of the rotational motion of the flow, which reduces (Nu). Therefore, it can be concluded that the natural convection phenomena inside the F-cavity can be controlled and depressed efficiently by using a magnetic field. As mentioned, it can be observed also that the peak value of (Nu) corresponds to (AR=0.2). Moreover, Fig. 12 shows that (Nu) decreases as (n) increases. Therefore, (Nu) reaches its peak value at (Ha=0 and n=0.6). Fig. 13 illus-



(a) AR=0.1 (b) AR=0.2

(c) AR=0.3 (d) AR=0.4

Fig. 11. The changes of (Nu) in terms of (n, φ and AR) at (Ra=10^6, Da=0.001, Ha=30 and λ=0.5).

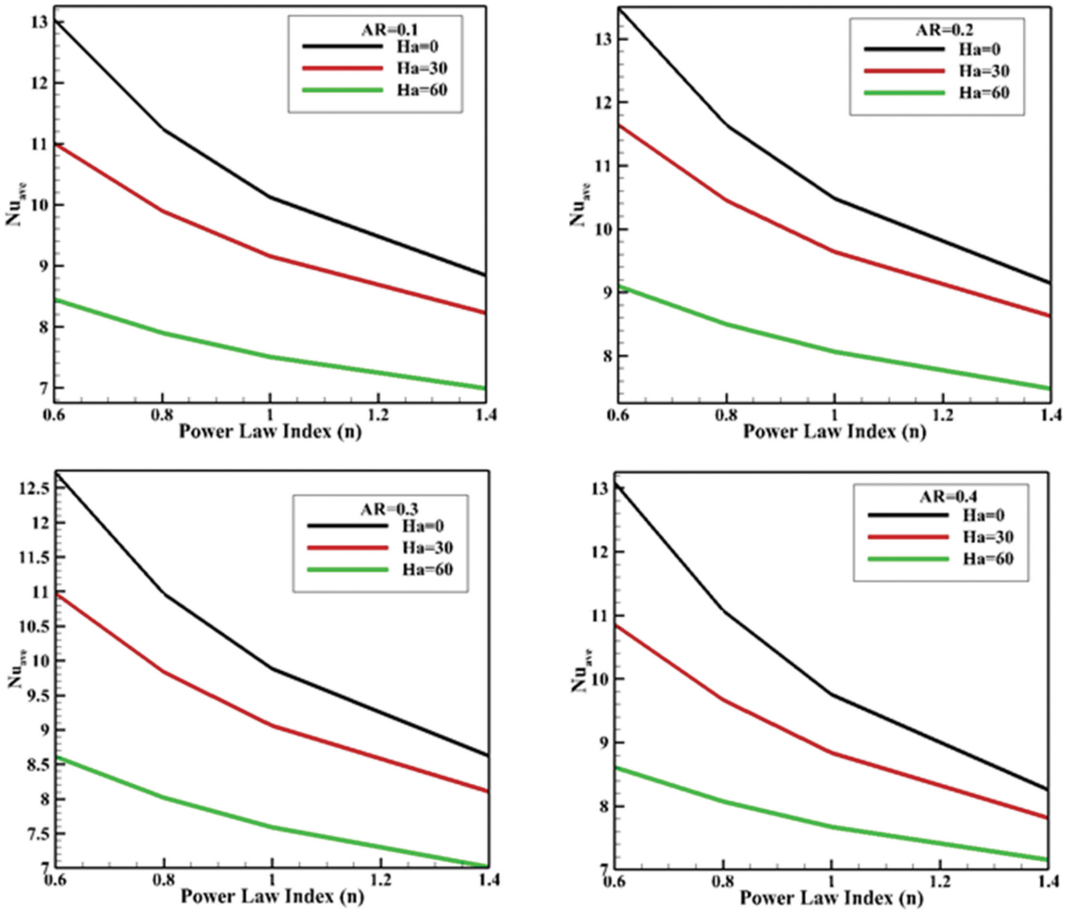


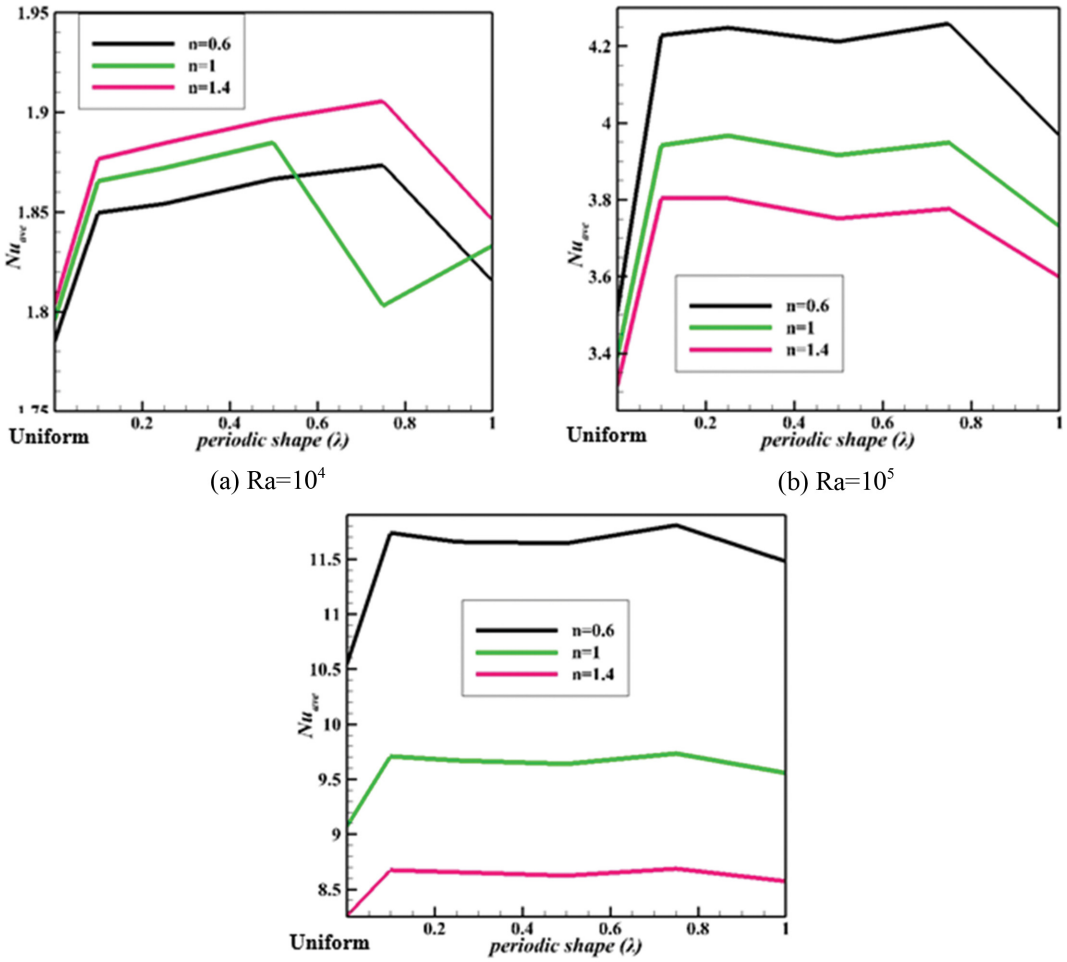
Fig. 12. The changes of (Nu) in terms of (Ha, n and AR) at (Ra=10^6, φ=0.04, Da=0.001 and λ=0.5).

trates (Nu) versus (λ, n and Ra) at (AR=0.2, Da=0.001, φ=0.04 and Ha=30). It is seen that (Nu) increases with the increase of (Ra). This can be related to the increase in the strength of vortices by boosting the buoyancy force. Improving (Ra) enhances the motion of the fluid and, therefore, intensifies the temperature gradient in the vicinity of the hot left sidewall, which results in an increase in the convection coefficient and, consequently, in (Nu). Besides, it is observed that (Nu) begins to augment linearly at (λ=0). This boosting trend continues until (λ) reaches (0.1). After that, the relationship between (Nu) and (λ) exhibits a different behavior depending on the considered (Ra). At (Ra=10^4), (Nu) increases by increasing (λ) for both the case of (n>1 and n<1) until it reaches (λ=0.75) and then begins to decline. While for the Newtonian (NF, i.e., n=1), it increases until (λ) reaches (0.5) and then decreases until (λ=0.75). After that, it rises again to (λ=1). At (Ra=10^5 and 10^6), (Nu) rises linearly with the growth of (λ) until (λ=0.1). After that, it decreases for all the considered values of (n). The only difference which can be noted is that the gap between the variations is increased at (Ra=10^6) compared with their corresponding variations at (Ra=10^5).

CONCLUSIONS

The goal of this numerical investigation was to analyze a naturally cooled F-shaped cavity containing aqueous Ag non-Newtonian (NF) saturated with a porous medium and subjected to a horizontal periodic magnetic field. The effects of (Ha, n, λ, Ra, AR, Da and φ) on the findings were evaluated. The following conclusions can be drawn from the results:

- The strength of the flow circulation decreases by boosting the (n) and (AR), whereas it increases by boosting (Da) and (Ra).
- The convective heat transfer mechanism inside the cavity is dominant when (Da) and (Ra) are high and (AR) is low.
- The strength of isotherms next to the hot left sidewall begins to drop with increasing (n).
- The flow field pattern is affected significantly by boosting the (λ).
- The isotherm lines are clearly affected by the variation of (λ). They change their pattern from curved shape to linear. Thus, convective heat transfer is dominant when ($0.25\leq\lambda\leq0.5$), whereas conduction is dominant when ($0.75\leq\lambda\leq1$).
- The minimum value of flow circulation strength occurs at (=1) for all the considered (n) values.
- (Nu) increases when (φ, Da and Ra) increase, whereas it decreases with the increase of (n) and (Ha).
- The highest value of (Nu) occurs at (AR=0.2).
- The relationship between (Nu) and (λ) exhibits a different behavior depending on the considered values of (Ra) and (n).



(a) Ra=10^4 (b) Ra=10^5

(c) Ra=10^6

Fig. 13. The changes of (Nu) in terms of (λ, n and Ra) at (AR=0.2, Da=0.001, φ=0.04 and Ha=30).

ACKNOWLEDGEMENTS

The first author would like to very thank Mrs. Topsy N. Smalley from United States of America for her kind assistance in completing this work.

NOMENCLATURE

AR : aspect ratio (H/L) [-]
$\vec{B}$: magnetic strength [Tesla]
B_o : amplitude of magnetic strength [Tesla]
C_p : specific heat capacity [kJ/kg·K]
Da : Darcy number [-]
F : coefficient of weight function
g : gravitational acceleration [m/s^2]
H : step length [m]
Ha : Hartmann number [-]
J : Jacobian of residual equation
k : thermal conductivity [W/m·K]
K : permeability of porous medium [m^2]
L : length & height of the cavity [m]
m : total number of nodes [-]
N : consistency coefficient [kg/m·s]
n : power-law index [-]
$\dot{P}$: dimensionless pressure [-]
$\dot{p}$: pressure [Pa]
Pr : Prandtl number [-]
Ra : Rayleigh number [-]
$\dot{T}$: temperature [K]
Nu_l : local Nusselt number [-]
Nu_{ave} : average Nusselt number [-]
$\dot{U}$: Dimensionless x-direction velocity component [-]
$\dot{u}$: x-direction velocity component [m/s]
$\dot{V}$: dimensionless y-direction velocity component [-]
$\dot{v}$: y-direction velocity component [m/s]
X, Y : dimensionless coordinate [-]
x, y : cartesian coordinates [m]

Greek Symbols

α : thermal diffusivity [m^2/s]
$\dot{\theta}$: dimensionless temperature [-]
λ : period number

Ψ : dimensionless stream function
μ : dynamic viscosity [kg/m·s]
σ : electrical conductivity [S/m]
ν : kinematic viscosity ($\dot{\nu}=\frac{\mu}{\rho}$) [$m^2/s$]
φ : nanoparticle volume fraction [%]
$\dot{\tau}$: shear stress tensor
$\emptyset$: basic function
β : thermal expansion coefficient [1/K]
ρ : density [kg/m^3]

Subscripts

c : cold
bf : base fluid (pure)
sp : solid particle
na : nanofluid
so : conductive solid cylinder
h : hot

Abbreviations

Cond. : Conduction
Conv. : Convection

REFERENCES

1. M. Ben Hamida, J. Belghaeib and N. Hajji, *Ther. Sci.*, **22**, 3107 (2018).
2. M. Massoudi, M. Ben Hamida and M. Almeshaal, *IJNMHFF*, **31**, 933 (2020).
3. M. Ben Hamida and K. Charrada, *Num. Heat Trans. - Part A*, **67**, 902 (2014).
4. R. Chand, G. Rana and A. K. Hussein, *Jou. of App. Flu. Mech.*, **8**, 265 (2015).
5. R. Chand, G. Rana and A. K. Hussein, *Inter. Jou. of Fluid Mech. Res.*, **42**, 390 (2015).
6. R. Kasmani, S. Sivasankaran, M Bhuvaneswari and A. K. Hussein, *IJNMHFF*, **27**, 2333 (2017).
7. A. K. Hussein, *Ren. and Sust. Ener. Rev.*, **42**, 460 (2015).
8. A. K. Hussein, *Ren. and Sust. Ener. Rev.*, **62**, 767 (2016).
9. M. Ben Hamida, J. Belghaeib and N. Hajji, *Arab. Jou. for Sci. and Eng.*, **43**, 4991 (2018).
10. R. Ben Jaballah, M. Ben Hamida, J. Saleh and M. Almeshaal, *IJNMHFF*, **29**, 3857 (2019).
11. M. Massoudi and M. Ben Hamida, *The Europ. Phys. Jou. Plus.*, **135**, 902 (2020).
12. S. Ahmed, A. K. Hussein, H. Mohammed, I. Adegun, X. Zhang, L. Kolsi, A. Hasanpour and S. Sivasankaran, *Nucl. Eng. and Des.*, **266**, 34 (2014).
13. S. Ahmed, A. K. Hussein, M. Abd El-Aziz and S. Sivasankaran, *Heat Trans. Res.*, **47**, 383 (2016).
14. T. Adekeye, I. Adegun, P. Okekunle, A. K. Hussein, S. Oyedepo, E. Adetiba and O. Fayomi, *Heat Trans.-Asi. Res.*, **46**, 261 (2017).
15. W. Pakdee, B. Yuvakanit and A. K. Hussein, *Jou. of Appl. Fluid Mech.*, **10**, 1153 (2017).
16. C. Maatki, K. Ghachem, L. Kolsi, A. K. Hussein, M. Borjini and H. Ben Aissia, *Appl. Math. and Comp.*, **273**, 178 (2016).
17. A. K. Hussein, H. Ashorynejad, S. Sivasankaran, L. Kolsi, M. Shikholeslami and I. Adegun, *Alex. Eng. Jou.*, **55**, 203 (2016).
18. M. Mahmoodi, *Inter. Jou. of Therm. Scien.*, **50**, 1731 (2011).
19. E. Sourtiji and S. Hosseinizadeh, *Therm. Scien.*, **16**, 489 (2012).
20. B. Mliki, M. Abbassi, K. Guedri and A. Omri, *Eng. Scie. and Tech., an Intern. Jou.*, **18**, 503 (2015).
21. N.Che Sidik and A. Safdari, *Adv. Mater. Res.*, **849**, 391 (2013).
22. N.Che Sidik and A. Safdari, *Jou. of Adva. Res. in Fluid Mech. and Therm. Scien.*, **21**, 1 (2016).
23. M. Mahmoodi and S. Hashemi, *Inter. Jou. of Therm. Scien.*, **55**, 76 (2012).
24. M. Mansour, M. Bakier and A. Chamkha, *IJNMHFF*, **24**, 1954 (2014).
25. R. Mohebbi, M. Izadi and A. Chamkha, *Phy. of Fluids*, **29**, 122009 (2017).
26. M. Mansour, A. Bakier and M. Bakier, *Amer. Jou. of Eng. Res.*, **2**, 49 (2013).
27. A. K. Hussein, M. Bakier, M. Ben Hamida and S. Sivasankaran, *Alex. Eng. Jou.*, **55**, 2157 (2016).
28. M. Izadi, R. Mohebbi, D. Karimi and M. Sheremet, *Chem. Eng. & Process.: Proc. Intens.*, **125**, 56 (2018).
29. R. Dehnavi and A. Rezvani, *Super. and Micros.*, **52**, 312 (2012).
30. A. Fard, P. Hooshmand, M. Mohammaei and D. Ross, *Therm. Scien. and Eng. Prog.*, **14**, 100373 (2019).
31. A. Purusothaman and E. Malekshah, *Therm. Scien. and Eng. Prog.*, **10**, 186 (2019).
32. A. Yadollahi, A. Khalesidoost, A. Kasaeipoor, M. Hatami and D. Jing, *The Europ. Phys. Jou. Plus.*, **132**, 372 (2017).
33. A. K. Hussein and A. Mustafa, *Heat Trans.-Asi. Res.*, **47**, 320 (2018).
34. A. K. Hussein and A. Mustafa, *Therm. Scien. and Eng. Prog.*, **1**, 66 (2017).
35. G. Kefayati, *Powd. Tech.*, **273**, 176 (2015).
36. G. Kefayati, *Powd. Tech.*, **127**, 176 (2016).
37. G. Kefayati, *Inter. Jou. of Heat and Mass Trans.*, **92**, 1066 (2016).
38. L. Wang , Z. Chai and B. Shi, *Inter. Jou. of Heat and Mass Trans.*, **102**, 381 (2016).
39. L. Wang, Z. Chai and B. Shi, *Adv. in Appl. Math. and Mech.*, **9**, 1094 (2017).
40. G. Kefayati and N. Che Sidik, *Powd. Tech.*, **305**, 679 (2017).
41. Z. Raizah, A. Aly and S. Ahmed, *Inter. Jou. of Mech. Scien.*, **140**, 376 (2018).
42. Q. Al-Amir, S. Ahmed, H. Hamzah and F. Ali, *Arab. Jou. for Scien. and Eng.*, **44**, 10339 (2019).
43. M. Jabbar, S. Ahmed, H. Hamzah, F. Ali and S. Khafaji, *Inter. Jou. of Mech. and Mechatr. Eng.*, **19**, 26 (2019).
44. L. Wang, C. Huang, X. Yang, Z. Chai and B. Shi, *Inter. Jou. of Heat and Mass Trans.*, **128**, 688 (2019).
45. A. Alsabery, A. Chamkha, S. Hussain, H. Saleh and I. Hashim, *Adv. Powd. Tech.*, **26**, 1230 (2015).
46. A. Alsabery, A. Chamkha, H. Saleh and I. Hashim, *Powd. Tech.*, **308**, 214 (2017).
47. M. Hatami, *Inter. Jou. of Heat and Tech.*, **36**, 509 (2018).
48. S. Acharya and S. Dash, *Num. Heat Trans. - Part A*, **76**, 552 (2019).
49. M. Massoudi, M. Ben Hamida, H. Mohammed and M. Almeshaal, *Energy*, **13**, 3457 (2020).
50. M. Massoudi and M. Ben Hamida, *Heat Trans.*, **50**, 2849 (2021).

51. B. Ruhani, D. Toghraie, M. Hekmatifar and M. Hadian, *Phys. A: Stat. Mech. and its Appl.*, **525**, 741 (2019).
52. S. Nazari, R. Ellahi, M. Sarafraz, M. Safaei, A. Asgari and O. Akbari, *Jou. of Therm. Analy. and Calor.*, **140**, 1121 (2020).
53. F. Soltani, D. Toghraie and A. Karimipour, *Powd. Tech.*, **371**, 37 (2020).
54. S. Dabiri, E. Khodabandeh, A. Poorfar, R. Mashayekhi, D. Toghraie and S. Abadian Zade, *Energy*, **153**, 17 (2018).
55. Y. Peng, A. Zahedidastjerdi, A. Abdollahi, A. Amindoust, M. Bahrami, A. Karimipour and M. Goodarzi, *Jou. of Therm. Analy. and Calor.*, **139**, 2623 (2020).
56. Y. Peng, A. Parsian, H. Khodadadi, M. Akbari, K. Ghani, M. Goodarzi and Q. Bach, *Phys. A: Stat. Mech. and its Appl.*, **549**, 124015 (2020).
57. A. Arani, O. Akbari, M. Safaei, A. Marzban, A. Alrashed, G. Ahmadi and T. Nguyen, *Inter. Jou. of Heat and Mass Trans.*, **113**, 780 (2017).
58. A. Malvandi, M. Safaei, M. Kaffash and D. Ganji, *Jou. of Magn. and Magn. Mater.*, **382**, 296 (2015).
59. R. Fatehi, A. Rahmat, N. Tofighi, M. Yildiz and M. Shadloo, *Comp. & Flus.*, **185**, 22 (2019).
60. M. Hopp-Hirschler, M. Shadloo and U. Nieken, *Comp. & Flus.*, **176**, 1 (2018).
61. M. Hemmat Esfe, M. Rejvani and D. Toghraie, *Case Stud. in Therm. Eng.*, **28**, 101437 (2021).
62. X. Li, S. Saeed, M. Beni, M. Morovvati, S. Angili, D. Toghraie, A. Khandan and A. Khan, *Compos. Scien. and Tech.*, **214**, 108973 (2021).
63. C. Ho, K. Lin, S. Rashidi, D. Toghraie and W. Yan, *Jou. of Molec. Liqs.*, **321**, 114760 (2021).
64. R. Abedinzadeh, E. Norouzi and D. Toghraie, *Jou. of Mater. Res. and Tech.*, **15**, 3481 (2021).
65. W. Qian, M. Vahid, Y. Sun, A. Heidari, R. Barbaz-Isfahani, S. Samandari, A. Khandan and D. Toghraie, *Jou. of Mater. Res. and Tech.*, **12**, 1931 (2021).
66. S. Aghakhani, B. Ghasemi, A. Hajatzadeh Pordanjani, S. Wongwises and M. Afrand, *Inter. Jou. Num. Meth. for Heat & Fluid Flow*, **29**, 4 (2019).
67. S. Aghakhani, A. Pordanjani, M. Afrand, M. Sharifpur and J. Meyer, *Inter. Jou. of Mech. Scien.*, **174**, 105470 (2020).
68. A. Hajatzadeh Pordanjani, S. Aghakhani, M. Afrand, B. Mahmoudi, O. Mahian and S. Wongwises, *Ener. Conv. and Manag.*, **198**, 111886 (2019).
69. A. Pordanjani and S. Aghakhani, *Heat Trans. Eng.*, In press (2021).
70. A. Pordanjani, S. Aghakhani, M. Afrand, M. Sharifpur, J. Meyer, H. Xu, H. Ali, N. Karimi and G. Cheraghian, *Jou. of Clean. Prod.*, **320**, 128573 (2021).
71. J. Reddy, *An introduction to the finite element method*, McGraw-Hill Inter. Edition, New York (1984).
72. G. Kefayati, *Inter. Jou. of Heat and Mass Trans.*, **112**, 709 (2017).